

Multiplexing Natural Orientation: Oppositely Directed Self-Assembling Peptides

Woo-jin Jeong,[†] Sanghun Han,[†] Hyeseo Park,[‡] Kyeong Sik Jin,[§] and Yong-beom Lim*,[†]

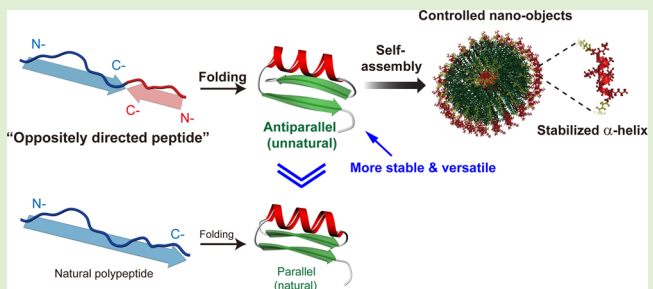
[†]Translational Research Center for Protein Function Control and Department of Materials Science & Engineering, Yonsei University, Seoul 120-749, Korea

[‡]Center for Research Facilities, Yonsei University, Seoul 120-749, Korea

[§]Pohang Accelerator Laboratory, Pohang University of Science and Technology, Pohang 790-784, Korea

Supporting Information

ABSTRACT: We explore here the possibility that polypeptide chains with directional multiplicity might provide for the control of peptide self-assembly processes. We tested this new possibility using an oppositely directed peptide (ODP) supramolecular system. The ODP could make it possible to form a $\beta\alpha\beta$ motif with antiparallel β -sheets, which does not exist in nature. Furthermore, the designed ODPs were able to self-assemble into discrete, homogeneous, and structured protein-like controlled nano-objects. ODPs represent a simple but powerful unnatural self-assembling peptide system that can become a basic scaffold for fabricating more complex and elaborate artificial nanostructures.



INTRODUCTION

Proteins are highly elaborate materials with a myriad of specialized functions. From the perspective of artificial systems, one of the most fundamental challenges is the development of protein-like synthetic materials that can mimic the structural and functional characteristics of natural proteins or perform novel functions that do not exist in nature. Self-assembled peptide nanostructures have gained much attention due to the possible fabrication of nanostructures that can mimic the structural and functional properties of proteins using peptide supramolecular building blocks, which are smaller in molecular size than proteins.^{1,2} On the other hand, the small peptide size can also be a weakness because of the difficulty in constructing sophisticated materials. To circumvent the inherent limitations of simple peptides, many chemical and structural modification strategies, such as lipidation, polymer conjugation, and cyclization have been developed.^{3–9}

Polypeptide chains in natural proteins always run in an N- to C-terminal direction, an unavoidable dogma that natural proteins have to follow. The $\beta\alpha\beta$ motif consists of an α -helix connected to a pair of β -strands (Figure 1a).¹⁰ Due to the compulsory N- to C- directionality of the natural polypeptide chain, only the formation of parallel β -sheets is allowed in a $\beta\alpha\beta$ motif for crossover connections with the α -helix.

Antiparallel β -sheets are substantially different from parallel sheets, and they have many advantageous properties over the latter.¹¹ Antiparallel β -sheets are typically more stable than parallel β -sheets because the former allows interstrand hydrogen bonds between carbonyls and amines to become more planar than the latter (Figure 1b).^{12–14} Additionally,

antiparallel β -sheets are also found to occur more abundantly than parallel sheets in proteins.^{12,14} Antiparallel β -sheets often consist of just two strands, whereas parallel β -sheets usually contain more than five total strands.¹⁵ Moreover, antiparallel β -sheets possess conformational degrees of freedom that allow them have a greater diversity in their spatial configuration than parallel β -sheets.^{15,16} Parallel β -sheets cannot tolerate solvent exposure on any side; therefore, they are always thoroughly buried within protein interiors with other structural layers on both sides.¹⁷ In contrast, antiparallel β -sheets can exist anywhere in proteins.

Probably one of the best ways to overcome the limitations of peptide supramolecular building blocks is to explore the possibility that is absent in natural protein systems and to make good use of the fact that peptides are chemically manageable. We envisioned that the introduction of multiplicity to the natural direction might give a new avenue for controlling peptide self-assembly processes. The $\beta\alpha\beta$ motif was used as a basic structural model to test our multiple directionality design principle. Here, we addressed the question of whether the introduction of directional multiplicity in polypeptide chain orientation could provide advantages over a singly oriented natural polypeptide and make it possible to produce novel protein folds that do not exist in natural systems.

Received: February 27, 2014

Revised: April 22, 2014

Published: April 29, 2014



EXPERIMENTAL SECTION

Materials. Fmoc amino acids were purchased from Novabiochem. The oligoethylene glycol-based linker N-(Fmoc-8-amino-3,6-dioxaoctyl) succinamic acid (Fmoc-PEG2-Suc-OH) was obtained from AnaSpec.

Peptide Synthesis. Peptides were synthesized on Rink Amide MBHA resin LL (Novabiochem) using standard Fmoc protocols in a

Tribute peptide synthesizer (Protein Technologies, Inc.). Standard amino acid protecting groups were employed with the exception of lysine, for which an *N*-[1-(4,4-dimethyl-2,6-dioxocyclohex-1-ylidene)-ethyl] (Dde) group was used. Deprotection of Dde from Dde-Lys(Fmoc)-OH was performed in 2% hydrazine in DMF. For cleavage and final deprotection, the resin was treated with a cleavage cocktail (TFA:1,2-ethanedithiol:thioanisole; 95:2.5:2.5) for 3 h and triturated

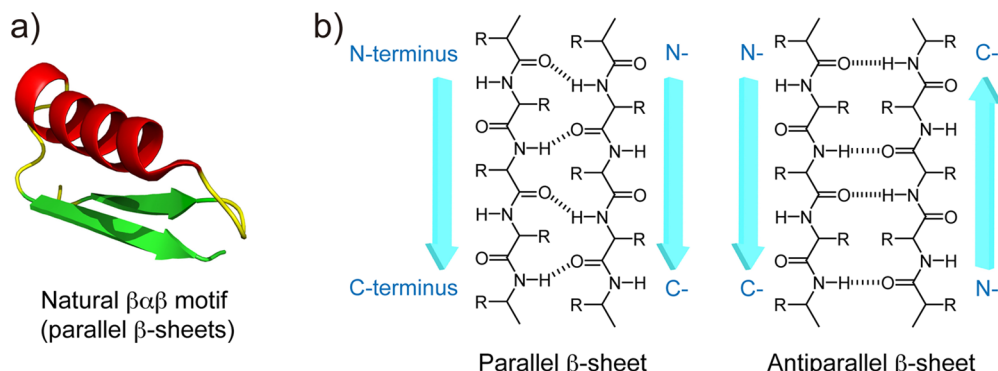


Figure 1. Parallel vs antiparallel. (a) An example of a natural $\beta\alpha\beta$ motif (PDB ID: 2HF3, monomeric actin). (b) Hydrogen bonding pattern of parallel vs antiparallel β -sheets.

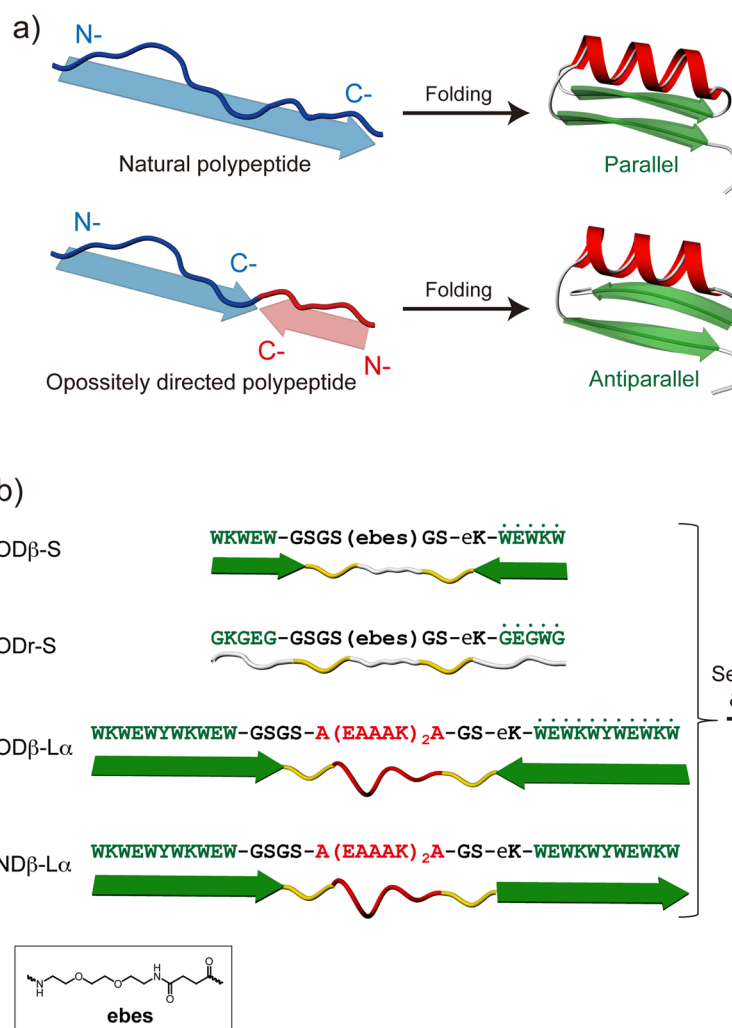


Figure 2. Design of oppositely directed supramolecular system. (a) Comparison of a naturally directed polypeptide (NDP) and an oppositely directed polypeptide (ODP). (b) Sequences and schematic diagrams for the self-assembling peptides used in this study. Oppositely directed amino acid residues are annotated with overhead dots. For the full chemical structures, see the Supporting Information.

with *tert*-butyl methyl ether (TBME). The peptides were purified by reverse-phase HPLC (water–acetonitrile with 0.1% TFA), and the molecular weight was confirmed by MALDI-TOF mass spectrometry. The purity of the peptides was >95%, as determined by analytical HPLC. The peptide concentration was spectrophotometrically determined in water/acetonitrile (1:1) urea using a molar extinction coefficient of tryptophan ($5,500 \text{ M}^{-1}\text{cm}^{-1}$) at 280 nm or an amide bond ($200 \text{ M}^{-1}\text{cm}^{-1}$) at 230 nm.

Circular Dichroism (CD) Spectroscopy. CD spectra were recorded using a Chirascan Circular Dichroism spectrometer equipped with Peltier temperature controller (Applied Photophysics, Ltd.). CD spectra for peptides were recorded from 260 to 190 nm using a 2 mm path-length cuvette. The CD spectrum was deconvoluted using the CDSSTR algorithm on the DICHROWEB online server.^{18,19} Reference data set 7 was used for the deconvolution. The total α -helix and β -sheet contents were calculated by adding the helix1 and helix2 and the strand1 and strand2 values, respectively.^{20,21}

Transmission Electron Microscopy (TEM). One microliter of sample was placed on a carbon-coated copper grid and dried completely. Next 2 μL of 2% (w/v) uranyl acetate solution was added for 1 min, and excess solution was wicked off using filter paper. The specimen was observed with a JEOL-JEM 2010 instrument operating at 120 kV. The data were analyzed using DigitalMicrograph software.

Atomic Force Microscopy (AFM). For AFM, typically 2 μL of the sample in water was deposited onto a freshly cleaved mica surface and dried completely. The images were obtained in tapping mode with a Nanoscope IV instrument (Digital Instruments). AFM scans were taken at set point of 0.8–1 V, and the scanning speed was 1–2 Hz.

Dynamic Light Scattering (DLS). DLS experiments were performed at room temperature using an ALV/CGS-3 compact goniometer system equipped with a He–Ne laser operating at 632.8 nm. The detector optics employed optical fibers coupled to an ALV/SO-SIPD/DUAL detection unit, which employed an EMI PM-28B power supply and an ALV/PM-PD preamplifier/discriminator. The signal analyzer was an ALV-5000/E/Win multiple-tau digital correlator with 288 exponentially spaced channels. The scattering angle was 90°. The size distribution was determined using a constrained-regularization method.

Fourier Transform Infrared Spectroscopy (FT-IR). For FTIR measurements, 100 μL of the sample (50 μM in water) was cast from the solution onto a ZnSe window. Three thousand scans were acquired with a Bruker VERTEX 70 FTIR spectrometer.

Fluorescence Spectroscopy. The steady-state fluorescence spectra were recorded using a PerkinElmer LS-55 fluorescence spectrophotometer in 1 cm path length quartz cuvettes. To measure the fluorescence from tryptophan residues, we excited samples at 280 nm. Excitation and emission slits with a nominal bandpass of 5 nm were used for measurement. OD β -S and OD β -La concentrations were 1 and 0.5 μM , respectively. Thioflavin T (ThT) assay for critical aggregation concentration (CAC) determination was performed as follows. To an increasing concentration of peptide solution, ThT was added to a final concentration of 50 μM . The mixture was then incubated for 1 h. The fluorescence intensity was measured using excitation and emission wavelengths of 440 and 490 nm, respectively. Excitation and emission slits with a nominal bandpass of 5 nm were used for measurement.

Small-Angle X-ray Scattering (SAXS) and Wide-Angle X-ray Scattering (WAXS). X-ray scattering experiments were performed at the 4C SAXS II beamline (BL) of the Pohang Accelerator Laboratory (PAL). A light source from an In-vacuum Undulator 20 (IVU 20:1.4 m length, 20 mm period) of the Pohang Light Source II storage ring was focused with a vertical focusing toroidal mirror coated with rhodium and monochromatized with a Si (111) double crystal monochromator (DCM), yielding an X-ray beam wavelength of 0.675 Å. Samples were mounted in solution sample cells with a mica window that had a thickness of 10 μm , a volume of 50 μL , and an X-ray beam path length of 0.8 mm and irradiated for 30 s of exposure time at room temperature. Scattered radiations were acquired using a two-dimensional (2D) charge-coupled detector (Mar USA, Inc.) positioned 1 m ($0.04 \text{ \AA}^{-1} < q < 0.50 \text{ \AA}^{-1}$) and

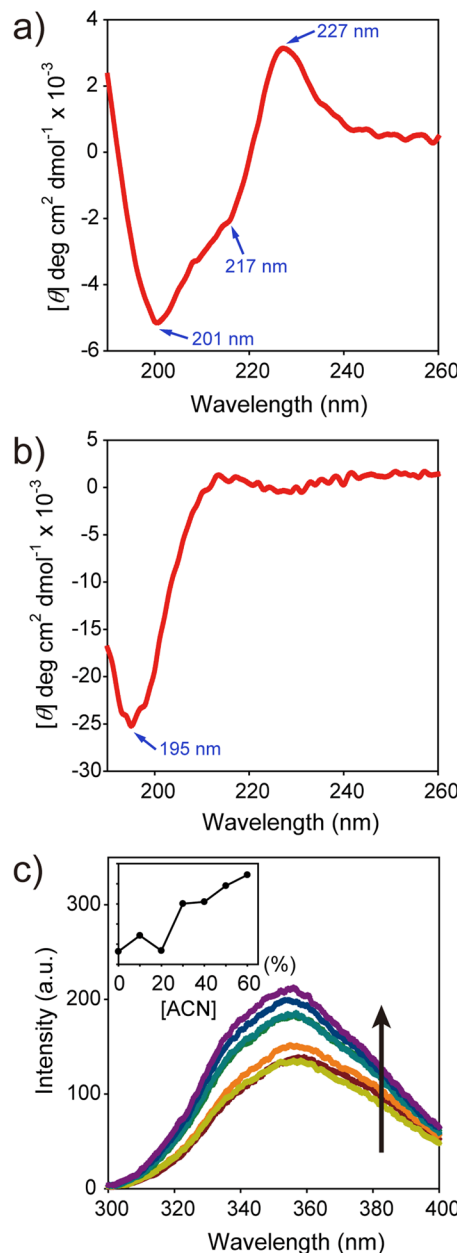


Figure 3. Characterization of the OD β -S peptide. CD spectra of (a) OD β -S and (b) ODr-S in water at room temperature (R/T). (c) Tryptophan fluorescence emission spectra of OD β -S at various ACN concentrations (0–60% relative to water, vol %). Inset: Plot of fluorescence intensities at tryptophan emission maxima (350 nm).

0.2 m ($0.21 \text{ \AA}^{-1} < q < 2.83 \text{ \AA}^{-1}$) away from the sample for SAXS and WAXS, respectively. The SAXS data were collected in five successive frames of 0.1 min each to minimize radiation damage. Each 2D SAXS pattern was circularly averaged from the beam center and normalized to the transmitted X-ray beam intensity, which was monitored with a scintillation counter placed behind the sample. The scattering of water was used as the experimental background. To determine structural information from the SAXS experimental curves, the pair distance distribution function $p(r)$ was obtained with the GNOM program²² using an indirect Fourier transform as follows:

$$p(r) = \frac{1}{2\pi^2} \int_0^\infty qrI(q)\sin(qr)dq$$

where q is the momentum transfer ($q = (4\pi/\lambda) \sin \theta$, where 2θ is the scattering angle and λ is the wavelength of the X-ray), and r is the distance

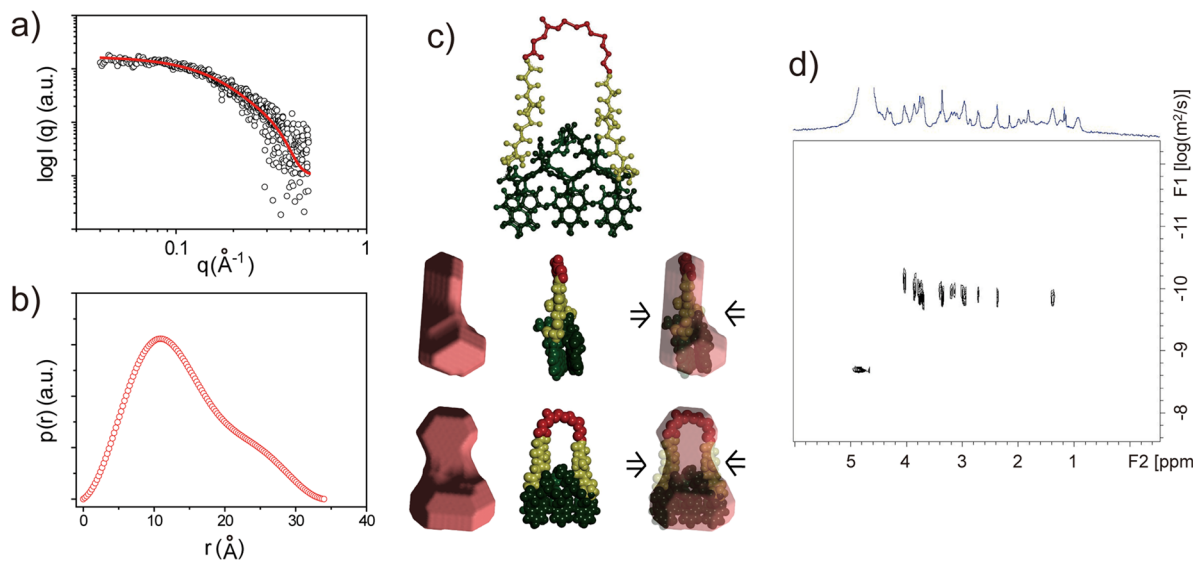


Figure 4. Characterization of the OD β -S peptide. (a) Small-angle X-ray scattering (SAXS) profiles of OD β -S in water at R/T. The open circles are experimental data and the solid line is the SAXS curve from a reconstituted model using an ab initio shape determination program, DAMMIF. (b) Pair Distance distribution function of OD β -S based on the experimental SAXS data using the program, GNOM. (c) Superimposition of the SAXS-derived molecular envelope with the molecular structure of OD β -S. (d) 2D DOSY spectrum of OD β -S in water.

between the paired scattering elements. Using this approach, the maximum diameter of a given macromolecule (D_{\max}) could be acquired from the distance where $p(r)$ converges to zero, and the radius of gyration ($R_{g,p(r)}$) could be calculated by the following equation:²³

$$R_{g,p(r)}^2 = \frac{\int r^2 p(r) dr}{2 \int p(r) dr}$$

The low-resolution ab initio shape of the peptide in water was reconstructed using the DAMMIF program²⁴ without any symmetry restriction. Surface rendering in the structural models was achieved using Discovery Studio 1.6 (Accelrys, Inc.).

Diffusion-Ordered NMR Spectroscopy (DOSY). DOSY NMR experiments were performed with 400 MHz Bruker Avance II NMR spectrometer. A pulse sequence using stimulated echo (STE) with bipolar gradient pulses and one spoil gradient was applied for 2D-DOSY experiments with a diffusion time (Δ) of 100 ms. The duration of the pulse-field gradient (δ) was optimized by performing a series of 1D diffusion experiments to obtain a residual signal less than 5% at the maximum gradient strength. The optimized δ was 2.0 ms. The pulse-field gradient (g) was increased in 64 steps ranging from 2 to 95% of the maximum gradient strength in a linear ramp. All measurements were performed at 298 K with a recycle time of 5 and 64 scans. An exponential window function with 1 Hz broadening was applied prior to the Fourier transformation. The diffusion coefficient of the peptide was determined using TopSpin 3.2 software (Bruker Biospin). From the obtained diffusion coefficient, the hydrodynamic radius (R_H) of the peptide was estimated using the Stokes–Einstein equation:

$$R_H = \frac{K_B T}{6\pi\eta D}$$

where K_B is the Boltzmann constant, T is the absolute temperature, η is the viscosity of the solvent, and D is the diffusion coefficient.

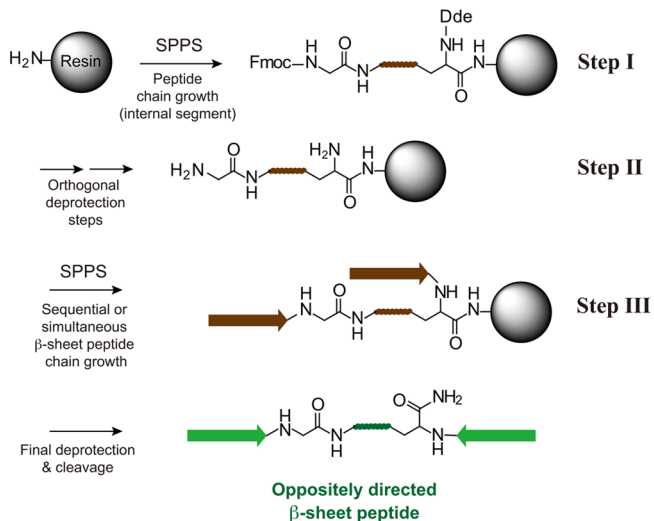
RESULTS AND DISCUSSION

With the reversal of chain direction in the second β -strand, we expected that the pair of β -strands in a $\beta\alpha\beta$ motif might be able to run in an antiparallel direction (Figure 2a). To test this hypothesis in the context of self-assembling peptides, we designed and synthesized β -sheet peptide supramolecular

building blocks that contain oppositely directed β -strands (Figure 2b). In our design, the β -sheet segments in peptide supramolecular building blocks consist of alternating repeats of hydrophobic/aromatic (tryptophan) and hydrophilic/charged (lysine or glutamic acid) amino acids, which have been shown to self-assemble via the formation of antiparallel β -sheets.^{25,26}

By combining the Fmoc solid-phase peptide synthesis (SPPS) protocol with an orthogonal deprotection scheme, a strategy for facile ODP chemical synthesis was devised (Scheme 1).

Scheme 1. Facile Route to Solid-Phase Synthesis of an Oppositely Directed β -Sheet Peptide^a



^aBrown, protected peptide segments; green, deprotected peptide segments.

The synthesis of ODPs such as OD β -S (oppositely directed β -sheet-short), ODr-S (oppositely directed random coil-short), and OD β -L α (oppositely directed β -sheet-large α -helix) begins with conventional SPPS of the internal segment (step I). Fmoc and Dde protection groups are located at the N- and C-terminus,

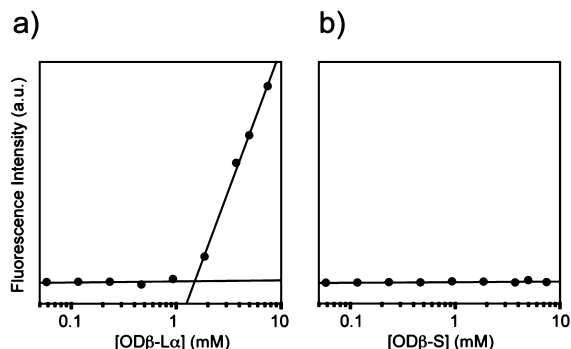


Figure 5. Changes in the ThT fluorescence as a function of (a) $\text{OD}\beta\text{-L}\alpha$ or (b) $\text{OD}\beta\text{-S}$ concentration.

respectively. These protection groups can be selectively deblocked due to their orthogonal properties (step II), allowing the sequential synthesis of two different peptide segments in opposite directions as in the case of ODr-S (step III). Alternatively, identical peptide segments in opposite directions can be simultaneously grown from the N- and C-terminus as in the case of $\text{OD}\beta\text{-S}$ and $\text{OD}\beta\text{-L}\alpha$ (step III).

To understand the folding and self-assembly behavior of ODPs in aqueous solution, we first used circular dichroism

(CD) spectroscopy to investigate the conformation of $\text{OD}\beta\text{-S}$, an ODP with short β -sheet-forming segments at both ends and an internal flexible segment. As shown in Figure 3a, the CD spectrum of $\text{OD}\beta\text{-S}$ is characterized by negative bands at 201 nm (random coil-like state, possibly due to the internal flexible segment) and 217 nm (β -sheet) and a positive band at 227 nm (an exciton-coupled band indicating interactions between aromatic chromophores²⁷), suggesting β -sheet formation and aromatic stacking between tryptophan residues. In contrast, ODr-S, an ODP without a β -sheet-forming segment, was found to be unordered without clearly defined secondary structures (Figure 3b). The aromatic stacking between tryptophan residues in $\text{OD}\beta\text{-S}$ was further supported by the fact that the emission intensity of tryptophan was gradually increased due to fluorescence dequenching as the acetonitrile (ACN) or urea concentration increased (Figures 3c and S5). ACN and urea was used to disrupt the hydrophobic and $\pi-\pi$ interactions between tryptophans.

Having demonstrated β -sheet formation and tryptophan interactions, the next question was whether this behavior had arisen as a result of intramolecular antiparallel β -sheet formation or intermolecular β -sheet formation (refer to Figure 7). To gain structural insight, we utilized SAXS to investigate the size and shape of $\text{OD}\beta\text{-S}$ in an aqueous solution. The scattering profile

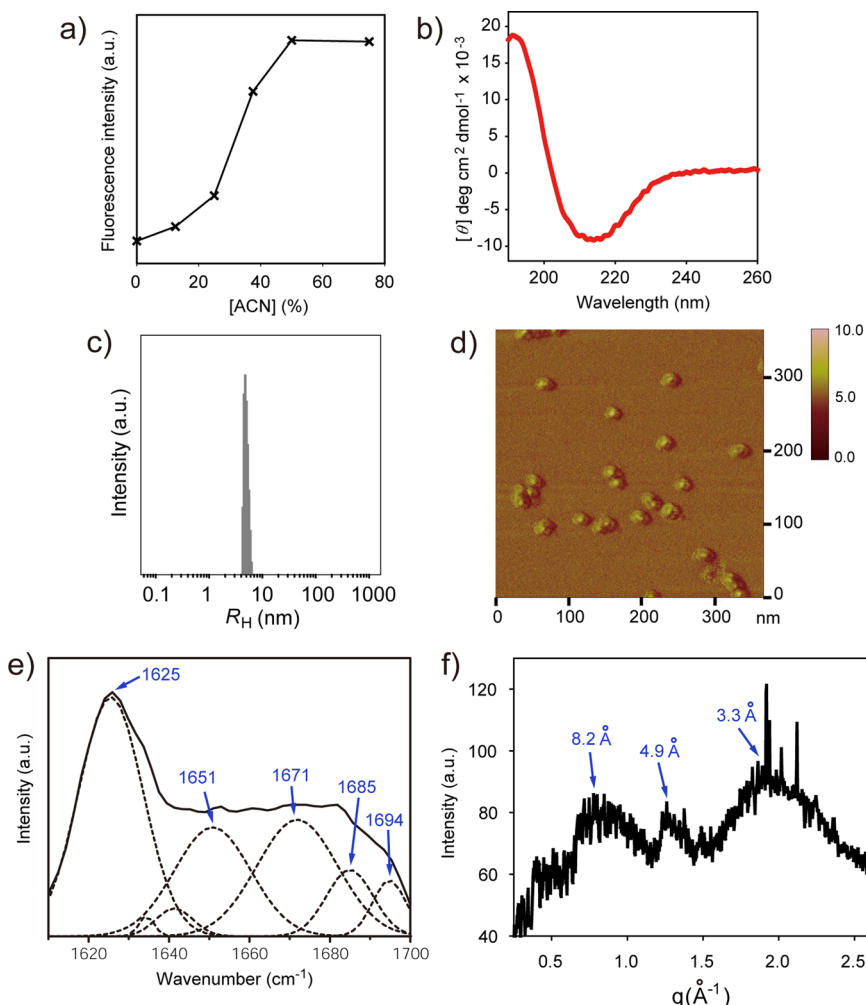


Figure 6. Characterization of the self-assembly behavior of the $\text{OD}\beta\text{-L}\alpha$ peptide. (a) Plot of tryptophan fluorescence at various ACN concentrations. $[\text{OD}\beta\text{-L}\alpha] = 0.5 \mu\text{M}$. CD spectrum (b), DLS data (c), AFM image (d), FTIR spectrum (e; dotted line, Fourier self-deconvolution analysis), and WAXS data (f) for $\text{OD}\beta\text{-L}\alpha$. All measurements were performed at R/T.

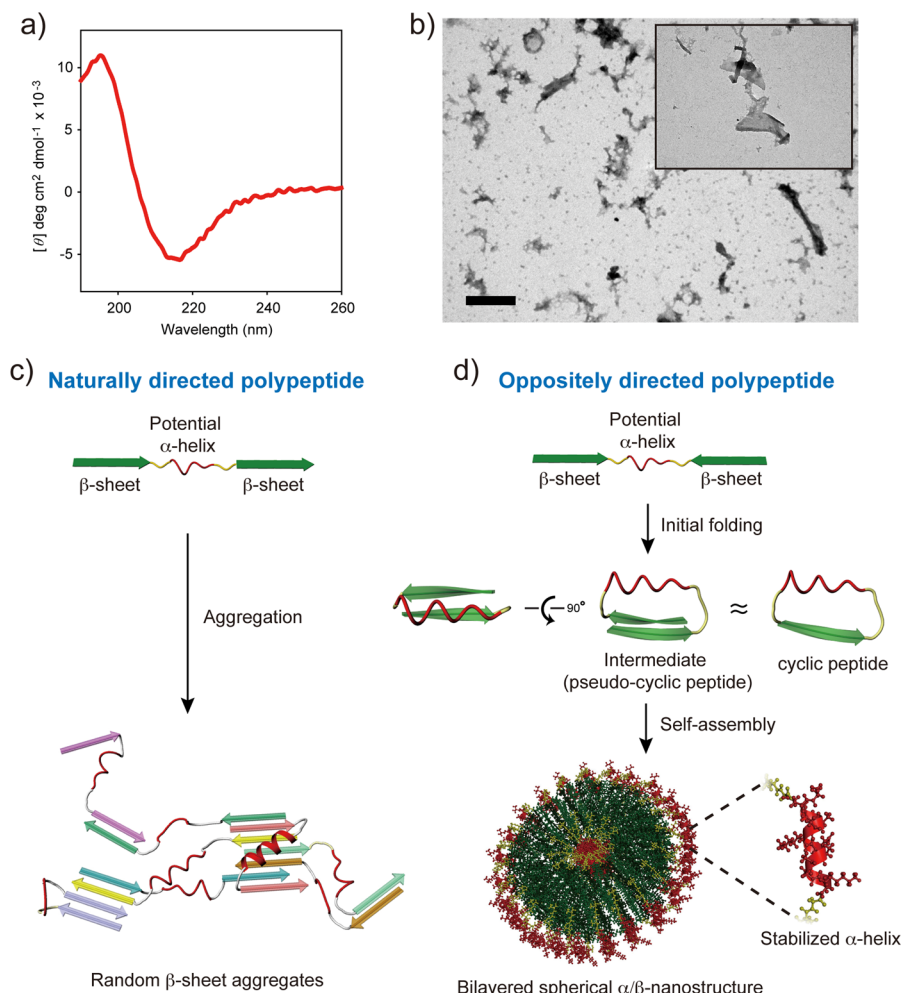


Figure 7. Comparison of the NDP and ODP systems. (a) CD spectrum of ND β -L α in water. (b) Negative-stain transmission electron microscopy (TEM) image of ND β -L α aggregates. Bar = 0.4 μ m. Inset: magnified image of the aggregates. Self-assembly pathways for NDPs (c) and ODPs (d).

of OD β -S is shown in Figure 4a. The scattering profile was analyzed using a pair distance distribution function $p(r)$, an expression of the scattering profile in real space (Figure 4b).^{23,28} This function can provide the radius of gyration, $R_{gp(r)}$, and the maximum dimension, D_{\max} . The calculation showed that the $R_{gp(r)}$ and D_{\max} for OD β -S are 11.01 ± 0.078 and 34.0 Å, respectively. The data suggest that OD β -S exists in a monomeric state rather than in an aggregated state. Moreover, a structural model reconstructed based on the SAXS data fits well with the molecular model of OD β -S with a monomeric intramolecular antiparallel β -sheet (Figures 4c and S7). We further confirmed the molecular dimension of OD β -S in aqueous solution using diffusion-ordered NMR spectroscopy (DOSY; Figure 4d).^{29,30} DOSY analysis showed that the hydrodynamic radius (R_H) of OD β -S is 12.27 Å ($D = 1.625 \times 10^{-10} \text{ m}^2/\text{s}$), which is consistent with the SAXS data. Taken together, all these data support the conclusion that OD β -S forms a monomeric pseudocyclic structure with an intramolecular antiparallel β -sheet.

We next designed an ODP with a longer β -sheet forming segment, OD β -L α , anticipating that the enhanced driving force for the β -sheet might induce oligomerization/self-assembly of the peptides in addition to the formation of a pseudocyclic structure. Additionally, an internal segment with a strong propensity toward an α -helix was incorporated to monitor its

conformational status during self-assembly. To investigate the self-assembly behavior of OD β -L α , thioflavin T (ThT) was employed as a spectroscopic probe. ThT binds to β -sheet-rich structures, such as amyloid fibrils, which lead to enhancement of the dye's fluorescence.³¹ As shown in Figure 5a, ThT fluorescence increased linearly with a gentle gradient to a certain point after which there was a sudden steep rise in fluorescence intensity. This result suggests β -sheet-mediated self-assembly of OD β -L α . The point of intersection of the extrapolated linear regression lines around the discontinuous point was used to calculate the critical aggregation concentration (CAC) of the peptide, which was found to be 1.5 μ M. In contrast, no such discontinuous change in ThT fluorescence was observed when OD β -S was used, further confirming the monomeric nature of the peptide (Figure 5b).

Another question regarding the self-assembly behavior of OD β -L α was whether the peptide has a tendency to form a pseudocyclic structure similar to that of OD β -S. To address this question, OD β -L α was diluted below its CAC value where the peptide exists in a monomeric state. As the concentration of ACN was increased, there was concomitant increase in tryptophan fluorescence due to a disruption in hydrophobic and $\pi-\pi$ stacking interactions between tryptophans, providing evidence for pseudocyclic structure formation (Figure 6a). Examination of the CD spectrum by deconvolution analysis

revealed the formation of α -helix (17%) and β -sheet (37%) in the OD β -L α assembly (Figure 6b).¹⁸

Dynamic light scattering (DLS) experiments revealed the formation of nanostructures with hydrodynamic radii (R_H) of ~ 5 nm (Figure 6c). Atomic force microscopy (AFM) examination revealed the formation of discrete and spherical nanostructures with diameters of ~ 15 – 18 nm (Figure 6d). The diameter of the nanostructures measured by AFM was slightly larger than that obtained by DLS, possibly due to the tip-broadening effect.³² As shown in Figure 6e, the Fourier transform infrared (FTIR) spectrum further confirmed the formation of a β -sheet (1625 cm^{-1}) and α -helix (1651 cm^{-1}). Additionally, bands at 1685 and 1694 cm^{-1} indicated that the β -strands were arranged in an antiparallel orientation. Self-assembled OD β -L α nanostructures were then characterized using wide-angle X-ray scattering (WAXS) in an aqueous solution. We found a reflection corresponding to *d*-spacings of 3.3 , 4.9 , and 8.2 \AA (Figure 6f). The peak at 3.3 \AA is characteristic of a π – π stacking distance, and 4.9 \AA corresponds to a β -sheet interstrand distance.^{33,34} The reflection at 8.2 \AA corresponds to the intersheet distance, suggesting the formation of bilayered structures (Figure 7d).

Taking all these data into consideration, ODPs have a strong tendency to form pseudocyclic structures through intramolecular antiparallel β -sheet interactions between oppositely directed β -sheet segments. The formation of α -helices in OD β -L α nanostructures suggests stabilization of the α -helices by a self-assembly induced coil-to-rod transition in the β -sheet segment and a subsequent molecular constraining effect.³⁵ Previously, α -helix stabilization by molecular constraining could be achieved when cyclic peptides were used.^{6,35–37} Thus, ODPs provide a facile linear peptide system that functions in a manner similar to cyclic peptides during self-assembly; however, ODPs are much easier to synthesize due to their linear topology (Figure 7d).

We then compared the oppositely directed peptide system with the naturally directed peptide system. The ND β -L α designed for this study was similar to OD β -L α except that the two β -sheet segments in the former peptide were aligned in the natural direction. CD investigation revealed that β -sheets were formed when ND β -L α was dissolved in an aqueous solution (Figure 7a). In contrast with OD β -L α , ND β -L α assembled into heterogeneous structures, frequently forming huge aggregates (Figure 7b). The results suggest that the intermolecular connections among ND β -L α molecules are multidirectional, resulting in the formation of irregular and large aggregates. The pseudocyclic intermediate is not likely to be formed by ND β -L α because β -sheets must lie in a less stable parallel direction. Therefore, the ND β -L α supramolecular building block with two β -sheet segments in the same direction assembles in a random bidirectional fashion (Figure 7c). However, the pseudocyclic structure of OD β -L α could have an enhanced orientational order, resulting in the formation of discrete and homogeneous self-assembled nanostructures (Figure 7d).

CONCLUSIONS

We were able to construct an unnatural $\beta\alpha\beta$ motif containing antiparallel β -sheets using an ODP system, which could further self-assemble into discrete nanostructures. The antiparallel $\beta\alpha\beta$ motif functions as a pseudocycle, enabling self-assembly-mediated molecular constraining and subsequent α -helix stabilization. Other advantages of the ODP system include the simplicity and ease of synthesis. The possibility of fabricating α -helix-decorated

controlled protein-like nano-objects using the ODP system further expands the diversity and potential of self-assembled peptide nanostructures.

ASSOCIATED CONTENT

Supporting Information

Synthetic scheme, chemical structures, mass spectra, HPLC chromatograms, additional fluorescence emission and CD spectra, and SAXS data. This material is available free of charge via the Internet at <http://pubs.acs.org>.

AUTHOR INFORMATION

Corresponding Author

*E-mail: yblim@yonsei.ac.kr; Tel.: +82-2-2123-5836; Fax: +82-2-312-5375.

Notes

The authors declare no competing financial interest.

ACKNOWLEDGMENTS

This work was supported by grants from the National Research Foundation (NRF) of Korea (2012R1A1A2006453, 2009-0083522, 2013M2B2A4041202, 2009-0066736).

REFERENCES

- (1) Fletcher, J. M.; Harmiman, R. L.; Barnes, F. R.; Boyle, A. L.; Collins, A.; Mantell, J.; Sharp, T. H.; Antognazzi, M.; Booth, P. J.; Linden, N.; Miles, M. J.; Sessions, R. B.; Verkade, P.; Woolfson, D. N. *Science* **2013**, *340*, 595–599.
- (2) Gazit, E. *Chem. Soc. Rev.* **2007**, *36*, 1263–1269.
- (3) Diegelmann, S. R.; Hartman, N.; Markovic, N.; Tovar, J. D. *J. Am. Chem. Soc.* **2012**, *134*, 2028–2031.
- (4) Hartgerink, J. D.; Beniash, E.; Stupp, S. I. *Science* **2001**, *294*, 1684–1688.
- (5) Shao, H.; Parquette, J. R. *Angew. Chem., Int. Ed.* **2009**, *48*, 2525–2528.
- (6) Jeong, W. J.; Choi, S. J.; Choi, J. S.; Lim, Y. B. *ACS Nano* **2013**, *7*, 6850–6857.
- (7) Hourani, R.; Zhang, C.; van der Weegen, R.; Ruiz, L.; Li, C.; Keten, S.; Helms, B. A.; Xu, T. *J. Am. Chem. Soc.* **2011**, *133*, 15296–15299.
- (8) Nagarkar, R. P.; Hule, R. A.; Pochan, D. J.; Schneider, J. P. *J. Am. Chem. Soc.* **2008**, *130*, 4466–4474.
- (9) Eckhardt, D.; Groenewolt, M.; Krause, E.; Borner, H. G. *Chem. Commun.* **2005**, 2814–2816.
- (10) Liang, H.; Chen, H.; Fan, K.; Wei, P.; Guo, X.; Jin, C.; Zeng, C.; Tang, C.; Lai, L. *Angew. Chem., Int. Ed.* **2009**, *48*, 3301–3303.
- (11) Cheng, P. N.; Pham, J. D.; Nowick, J. S. *J. Am. Chem. Soc.* **2013**, *135*, 5477–5492.
- (12) Perczel, A.; Gaspari, Z.; Csizmadia, I. G. *J. Comput. Chem.* **2005**, *26*, 1155–1168.
- (13) Zhao, Y. L.; Wu, Y. D. *J. Am. Chem. Soc.* **2002**, *124*, 1570–1571.
- (14) Richardson, J. S. *Nature* **1977**, *268*, 495–500.
- (15) Salemme, F. R. *Prog. Biophys. Mol. Biol.* **1983**, *42*, 95–133.
- (16) Salemme, F. R.; Weatherford, D. W. *J. Mol. Biol.* **1981**, *146*, 119–141.
- (17) Zubay, G. L. *Biochemistry*, 3rd ed.; Wm. C. Brown Publishers: Dubuque, IA, 1993.
- (18) Whitmore, L.; Wallace, B. A. *Nucleic Acids Res.* **2004**, *32*, W668–673.
- (19) Whitmore, L.; Wallace, B. A. *Biopolymers* **2008**, *89*, 392–400.
- (20) Breitinger, H. G.; Villmann, C.; Melzer, N.; Rennert, J.; Breitinger, U.; Schwarzsinger, S.; Becker, C. M. *J. Biol. Chem.* **2009**, *284*, 28624–28633.
- (21) Sreerama, N.; Venyaminov, S. Y.; Woody, R. W. *Protein Sci.* **1999**, *8*, 370–380.

- (22) Semenyuk, A. V.; Svergun, D. I. *J. Appl. Crystallogr.* **1991**, *24*, 537–540.
- (23) Kim, M.; Rho, Y.; Jin, K. S.; Ahn, B.; Jung, S.; Kim, H.; Ree, M. *Biomacromolecules* **2011**, *12*, 1629–1640.
- (24) Franke, D.; Svergun, D. I. *J. Appl. Crystallogr.* **2009**, *42*, 342–346.
- (25) Han, S.; Kim, D.; Han, S. H.; Kim, N. H.; Kim, S. H.; Lim, Y. B. *J. Am. Chem. Soc.* **2012**, *134*, 16047–16053.
- (26) Jeong, W. J.; Lee, M. S.; Lim, Y. B. *Biomacromolecules* **2013**, *14*, 2684–2689.
- (27) Cochran, A. G.; Skelton, N. J.; Starovasnik, M. A. *Proc. Natl. Acad. Sci. U.S.A.* **2001**, *98*, 5578–5583.
- (28) Putnam, C. D.; Hammel, M.; Hura, G. L.; Tainer, J. A. *Q. Rev. Biophys.* **2007**, *40*, 191–285.
- (29) Macchioni, A.; Ciancaleoni, G.; Zuccaccia, C.; Zuccaccia, D. *Chem. Soc. Rev.* **2008**, *37*, 479–489.
- (30) Binolfi, A.; Fernandez, C. O.; Sica, M. P.; Delfino, J. M.; Santos, J. *Proteins* **2012**, *80*, 1448–1464.
- (31) Xue, W. F.; Homans, S. W.; Radford, S. E. *Proc. Natl. Acad. Sci. U.S.A.* **2008**, *105*, 8926–8931.
- (32) Li, B. S.; Cheuk, K. K. L.; Salhi, F.; Lam, J. W. Y.; Cha, J. A. K.; Xiao, X.; Bai, C.; Tang, B. Z. *Nano Lett.* **2001**, *1*, 323–328.
- (33) Banerjee, A.; Palui, G.; Banerjee, A. *Soft Matter* **2008**, *4*, 1430–1437.
- (34) Xu, H.; Das, A. K.; Horie, M.; Shaik, M. S.; Smith, A. M.; Luo, Y.; Lu, X.; Collins, R.; Liem, S. Y.; Song, A.; Popelier, P. L.; Turner, M. L.; Xiao, P.; Kinloch, I. A.; Ulijn, R. V. *Nanoscale* **2010**, *2*, 960–966.
- (35) Lim, Y. B.; Moon, K. S.; Lee, M. *Angew. Chem., Int. Ed.* **2009**, *48*, 1601–1605.
- (36) Choi, S. J.; Jeong, W. J.; Kim, T. H.; Lim, Y. B. *Soft Matter* **2011**, *7*, 1675–1677.
- (37) Kim, B.; Choi, S. J.; Han, S. H.; Choi, K. Y.; Lim, Y. B. *Chem. Commun.* **2013**, *49*, 7617–7619.